THE JOURNAL OF PHYSICAL CHEMISTRY C

Article

pubs.acs.org/JPCC

Detailing Ionosorption over TiO_2, ZrO_2, and HfO_2 from First Principles

Juan C. Garcia and N. Aaron Deskins*

Department of Chemical Engineering, Worcester Polytechnic Institute, 100 Institute Road, Worcester, Massachusetts 01609, United States

ABSTRACT: Identifying the principles of surface to adsorbate charge transfer is key to a better understanding of metal oxide materials as both catalysts and gas sensors. The mechanism responsible for gas sensing effects is not fully understood, but is associated with electron transfer to adsorbates, forming negatively charged anions, or ionosorption. Catalytic surface reactions may also involve electron transfer from the oxide to the adsorbates. Using density functional theory, we modeled the adsorption of small molecules over stoichiometric and reduced metal oxide surfaces of group IV metals and quantify the effect of electron transfer upon adsorption. Surface reduction was accomplished through creation of oxygen vacancies, which lead to unpaired electrons within the oxide lattice, and which may eventually transfer to adsorbates. We examined the TiO_2 anatase (101), tetragonal HfO_2 (101), and tetragonal ZrO_2 (101) surfaces. We first focused on O_2 (a known electron scavenger) adsorption at surface cation sites and observed formation of anionic O_2 species, stabilizing O_2 on the surface. The ability of O_2 to scavenge electrons was found to be geometry-dependent, as electron transfer only occurred for a specific O_2 configuration, O_2 lying flat on the surface. We found a correlation between the work function of the metal oxide, and the ionic adsorption of the oxygen molecule; surfaces with smaller work function values have larger adsorption energies for O_2. The ionic character of a surface, as measured by vacancy formation energy, also correlates well with the O_2 adsorption energy. Thus, if the work function or vacancy formation energy of a metal oxide surface is known, it may be possible to predict when electron transfer occurs and to what degree during adsorption. By examining several other adsorbates (such as H_2O or CO), we found that charge transfer only occurs during the adsorption process of an adsorbate more electronegative than the surface, in agreement with previous work (Deskins et al. *J. Phys. Chem. C* **2010**, *114*, 5891−5897). Our results therefore do show that electron transfer does not occur with all adsorbates (i.e., those molecules with low electronegativity), but any studies involving these metal oxides should take into account the possibility of ionosorption due to unpaired electrons resulting from surface reduction (defects) to correctly describe the surface chemistry involving many typical compounds.

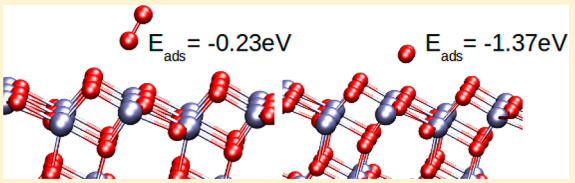

1. INTRODUCTION

The study of metal oxides is an area of rich active research, because some of the most interesting magnetic, optical, and electronic properties are found within this class of materials. Understanding the surface properties of metal oxides, their electronic structure, and reactivity with adsorbed molecules is crucial in many technological applications.[1] In addition, surface defects are highly important as they largely determine phenomena such as corrosion, adsorption, and catalytic behavior for many oxides. Defects often lead to excess electrons within the metal oxide lattice, or reduction of the material, and the ability of these electrons to affect surface chemistry has been the subject of several studies.[2−7]

Metal oxides are often used either as catalyst supports or directly as catalysts for a variety of applications.[8] Electron transfer from the metal oxide plays a fundamental role in many catalytic processes, such as photocatalytic oxidation of organic contaminants and other reactions over TiO_2.[9] Oxygen acts as a well-known electron scavenger in these processes, and without its presence the photocatalyst would deactivate due to negative charge accumulation.[4,10,11] Detection of gases is also a subject of growing importance with domestic, environmental, and industrial applications.[12] Metal oxides have attracted attention for gas sensing applications due to their sensitivity and relatively low cost. The design of better gas sensing devices depends in part on knowledge of the sensing mechanism. The gas sensing mechanism is associated with surface reactions of absorbed molecular and atomic ions (O_2^- and O^-) that have scavenged electrons and then can react with a reducing gas such as CO, releasing electrons.[13] After the adsorption of a molecule on the surface, the concentration of electrons in the conduction band decreases due to surface electron transfer, which leads to increased electrical resistance of the material. This process in turn leads to a change in the conductivity of the oxide, allowing the indirect detection of the gas.

These gas-sensing effects have been explained by the ionosorption model.[14] This is illustrated in Figure 1, which shows the initial adsorption, electron transfer, and final anionic state of the adsorbate. Electrons from the conduction band of the solid become captured by adsorbates, leading to ionization of the adsorbate, or anion formation. The bond formed in this process thus has strong ionic character, as the negatively charged adsorbate interacts with positively charged surface metal cations. SnO_2 sensors are the prototype oxide-based gas

Received: May 4, 2012
Revised: July 16, 2012
Published: July 17, 2012

dx.doi.org/10.1021/jp3043285 | *J. Phys. Chem. C* 2012, 116, 16573−16581

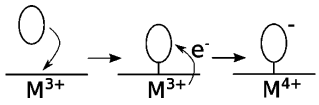

Figure 1. Illustration of the ionosorption process showing adsorption, then electron transfer to form an anionic adsorbate. M represents a metal cation site.

sensor involving ionosorption. There is however a great interest in understanding the mechanism in other oxides to develop better gas-sensing devices.[15−17]

Defects can have a strong effect on surface processes because they can provide electrons for charge-transfer processes, as shown in Figure 1. Defects can also serve directly as reaction sites, such as an oxygen vacancy being filled by H_2O or O_2, but the current work does not address the direct reactivity at these reaction sites. Rather, the role of defects as electron-donating centers is only considered. For instance, oxygen vacancies lead to a reduced surface with excess electrons, which introduce defect states in the band gap.[18] In TiO_2 for each removed oxygen atom, two electrons remain in the lattice of the Ti atoms, and two Ti^{4+} are reduced to Ti^{3+}. Other defects such as interstitial Ti atoms or H atoms also lead to unpaired electrons.[2−4,19] The reduction of the surface can change the adsorption energy of many atoms and molecules.[3,5,20,21] The current work concerns the transfer of unpaired electrons to adsorbates due to the presence of surface O vacancies (O_v), and what role these electrons play in adsorption and chemistry over group IV metal oxide surfaces.

Adsorption over TiO_2 has been extensively studied,[9,22−24] especially over the rutile phase. However, the anatase polymorph of TiO_2 is also a promising material because of its reactivity.[1,25] There are several theoretical studies on adsorption reactions and surface properties of anatase (101) surfaces.[26−29] DFT calculations also indicate that in the presence of O vacancies (O_v), several adsorbates have higher adsorption energies over anatase as compared to rutile, and the defects may act as nucleation sites for Au and Pt growth.[30] HfO_2 and ZrO_2 surfaces have been less studied than TiO_2, particularly using theoretical methods. However, significant attention has been paid to the deposition of thin zirconia/hafnia films for microelectronics and catalysis.[31−37] Theoretical studies of HfO_2 and ZrO_2 surface adsorption have been performed, such as involving water and hydrogen,[38−41] Au,[42] or sulfuric acid.[43] Surface defects have also been modeled,[44−46] although charge transfer due to the presence of point defects has not systematically been explored over these oxides.

Previous work by Deskins et al.[3] examined charge transfer over the rutile (110) surface with density functional theory (DFT). They found a correlation between the number of excess electrons and the strength of O_2 adsorption. The number of excess electrons in the surface was moderated by the number and type of defect (O vacancy, surface hydroxyl, or interstitial Ti atom). They also demonstrated that significant charge transfer occurs only for species with large electronegativities greater than the electronegativity of the rutile (110) TiO_2 surface. Other computational work also showed similar electron transfer events over the rutile (110) surface.[5,7]

In the present work, we examine charge transfer to adsorbates over reduced surfaces of the anatase phase of TiO_2, and tetragonal phases of HfO_2 and ZrO_2 (all group IV metal oxides) using DFT. We compare these three metal oxides and determine the details of electron transfer for them, including what factors influence charge transfer to adsorbates and on which surfaces electron transfer has the largest effect. We first examined O_2 adsorption, and then considered several other adsorbates. We provide several new insights that may be helpful for the future design and study of gas sensors and catalytic metal oxides.

2. METHODOLOGY

The DFT computations were performed with the CP2K[47,48] package. It uses the Gaussian and plane waves approach (GPW) with periodic boundary conditions. Valence electrons were described by a double-ζ basis set, specifically optimized to perform accurate molecular calculations. This basis set is well suited for the condensed phase.[49] Core electrons were described by Goedecker−Teter−Hutter (GTH) pseudopotentials.[50−52] Within the pseudopotential approximation, only valence electrons are represented explicitly in the calculations, with the valence-core interaction being represented by nonlocal pseudopotentials. The gamma point supercell approach was used, necessitating the use of large supercells. Calculations have been performed using the Perdew−Burke−Ernzerhof (PBE) functional for the exchange correlation term of the electron−electron interaction,[53] and all calculations were spin polarized.

Table 1 shows calculated and experimental bulk lattice parameters for the studied metal oxides. These lattice parameters were found using a 3 × 3 × 3 bulk lattice cell. Optimized bulk lattice parameters were found to agree well with experimental data; the maximum deviation was 1.9% for the a parameter of ZrO_2, while the other parameters showed deviations of less than 1%.

Table 1. Comparison of Calculated and Experimental Lattice Parameters for Tetragonal HfO_2 and ZrO_2, and Anatase TiO_2

	TiO_2	HfO_2	ZrO_2
a [Å]	3.76	3.62	3.57
a_{exp} [Å]	3.79	3.64	3.64
b [Å]	9.52	5.23	5.26
b_{exp} [Å]	9.54	5.27	5.29
experimental ref	54	55	56

Periodic slab models were used for all of the metal oxide surfaces. Each slab size was set to be (3 × 2) in the [011] and [010] directions, respectively, and six atomic layers thick with ~20 Å vacuum spacing between slabs. The total lateral size of each surface slab was 11.28 Å by 20.47 Å for anatase (101), 10.71 Å by 12.71 Å for HfO_2 (101), and 10.87 Å by 12.32 Å for ZrO_2 (101). Figure 2 shows the slab models used. The bottom O−M−O trilayer (three atomic layers) was kept fixed, and all other atoms were free to relax during optimization. Typically one surface O atom was removed to create a reduced surface.

To compare the reducibility of the surface, we computed the formation energy of an oxygen vacancy E_{vac} according to:

$$E_{vac} = E_{1/2O_2} + E_{reducedslab} - E_{cleanslab} \quad (1)$$

where $E_{1/2O2}$ is the energy of a oxygen atom computed as one-half of the energy of a oxygen molecule, $E_{reduced\ slab}$ is the energy of the metal oxide surface with an oxygen vacancy, and $E_{clean\ slab}$ is the energy of the stoichiometric slab. Positive energies indicate endothermic processes so that the energy of an oxygen vacancy is smaller for a more reducible surface. The work function, defined as the energy needed to move an electron

dx.doi.org/10.1021/jp3043285 | J. Phys. Chem. C 2012, 116, 16573−16581

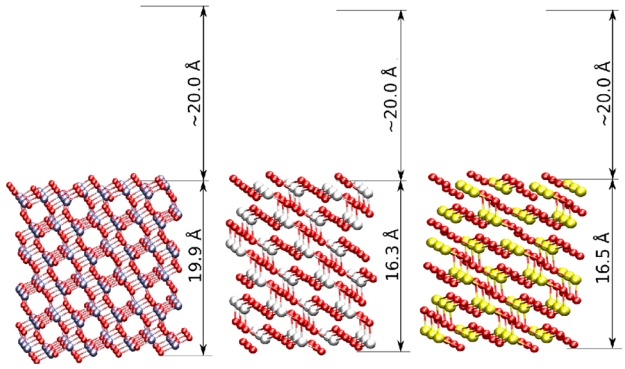

Figure 2. Slab models used in the current work. Surfaces of (a) anatase TiO_2 (101), (b) tetragonal ZrO_2 (101), and (c) tetragonal HfO_2 (101). Slab thicknesses are indicated as well as vacuum spacings. The red spheres represent oxygen, the blue spheres represent Ti, the white spheres Hf, and the yellow spheres represent Zr. The same color scheme is used in the remaining figures.

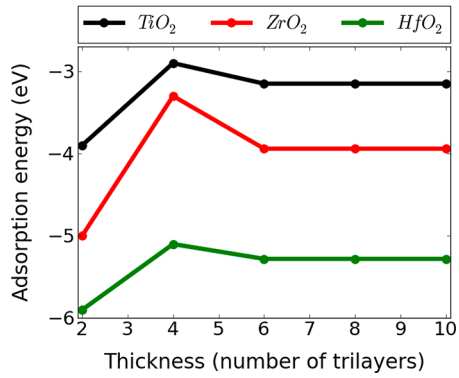

Figure 3. Convergence of the adsorption energy of O_2 over reduced surfaces of TiO_2, ZrO_2, and HfO_2 as a function of slab thickness. Each layer on the plot is an O−M−O trilayer, or three atomic layers.

from the Fermi level to vacuum, was computed for each metal oxide slab. This was done to roughly compare the surfaces' relative electronegativity. The methodology used was based on the method proposed by Fall.[57] For each reduced slab, we calculated the average electrostatic potential perpendicular to the surface as a function of the z coordinate value. This was used to establish the vacuum energy level, or the flat electrostatic region outside the slab. The work function was then found by taking the difference between the vacuum level and Fermi level (calculated from the eigenvalues).

Adsorption energies E_{ads} were calculated using the following expression:

$$E_{ads} = E_{surf+adsorbate} - E_{surf} - E_{adsorbate} \quad (2)$$

where $E_{adsorbate}$ is the energy of the isolated molecule in the vacuum, E_{surf} is the energy of the bare slab, and $E_{surf+adsorbate}$ is the total energy of the molecule adsorbed on the slab. We calculated adsorption energies over both stoichiometric and reduced surfaces. Bader charge analysis was performed to analyze the charge distribution.[58−61] For all of the adsorbates, we modeled the adsorption over the metal atoms, or the cationic sites, as opposed to over O atoms. Several adsorption geometry configurations were found for each adsorbate, but the most stable geometries are analyzed herein. Previous research found that the exact physical location of the defect relative to the adsorbate had little effect on the surface chemistry,[3] so we did not consider this matter further. Adsorbates were placed sufficiently far away from an O vacancy to preclude direct reactivity of adsorbates with the O vacancy; the O vacancy only serves to reduce the surface.

To confirm the validity of our model, we performed several convergence tests. We determined a suitable slab thickness by calculating the adsorption energy of O_2 (in the side-on configuration as discussed in section 3.2) as a function of slab thickness. The results, as shown in Figure 3, indicate that the adsorption energy is converged for six layers or larger (each layer being an O−M−O trilayer, or three atomic layers). We therefore used a six-layer slab in the current work.

The use of a single k-point may introduce errors in our calculations because of an insufficient k-point mesh. We tested this possibility by determining adsorption energies for slabs with larger dimensions in the x- and y-directions. By increasing the supercell size, the distance between k-points decreases, or k-point density increases. Convergence is reached when increasing the supercell shows little or no change in calculated properties. We calculated the adsorption energy of O_2 while changing the surface size, and the results are summarized in Table 2. Our results indicate that the use of a (3 × 2) surface cell gives sufficient k-point sampling.

Table 2. Adsorption Energy of O_2 [eV] over Stoichiometric Surfaces Using Different Surface Cell Sizes

	surface size		
metal oxide	3 × 2	3 × 3	4 × 3
TiO_2	−1.37	−1.37	−1.36
ZrO_2	−0.55	−0.54	−0.55
HfO_2	−1.36	−1.36	−1.35

3. RESULTS AND DISCUSSION

3.1. Nature of the Reduced Surfaces. Our reduced surfaces showed properties similar to those from previous research. Our calculated formation energy of an oxygen vacancy in the anatase (101) surface (4.87 eV) was similar to the value reported in previous DFT work (4.15 eV).[62] The slight difference in formation energy could be due to our larger slab as well as basis set or pseudopotential choice. For the (101) surface of tetragonal ZrO_2, our formation energy was calculated to be 7.14 eV, and previous DFT work reported a value of 8.4 eV.[63] This latter study used an embedded atom cluster approach. Another paper[19] calculated the value to be 5.48 eV, using the plane waves method, contrasted with the hybrid basis set method that we used. Both HfO_2 and ZrO_2 are less studied than TiO_2, so there are less available data on these two oxides. Still the literature thus reports O_v formation energies using a variety of methods and simulation parameters, and our calculated vacancy formation energies fit the range of reported values. We also comment that the calculated O_v formation energies may not be fully correct due to errors in DFT, but trends are likely to be valid due to systematic cancellation of errors in comparing two materials using the same level of theory.

Graphs of the spin density (the difference between the spin up and spin down densities) for the ZrO_2 and HfO_2 surfaces are shown in Figure 4. These graphs demonstrate the presence of unpaired electrons mainly localized on the 3d levels of the neighboring Hf and Zr atoms, which coincide with previous

dx.doi.org/10.1021/jp3043285 | J. Phys. Chem. C 2012, 116, 16573−16581

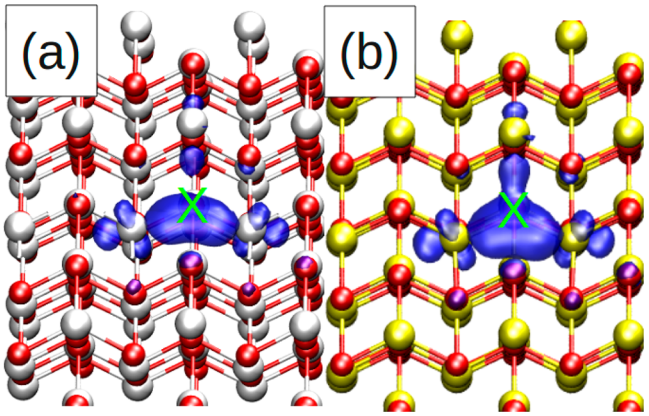

Figure 4. Spin density plots in the region near the oxygen vacancies of the surfaces (a) t-ZrO_2 (101) and (b) t-HfO_2 (101). The location of an oxygen vacancy is indicated by an X.

work.[64−66] The DFT method did not show localized electrons on the anatase surface. The GGA approach tends to delocalize the electrons in TiO_2;[18,19] this is a known limitation that can be avoided with the DFT+*U* method, which will be discussed later. Our results in modeling reduced surfaces indicate that our simulation approach is in adequate agreement with previous DFT work, and that our approach is therefore reasonable.

3.2. Adsorption of O_2. We used molecular oxygen as a prototype molecule for our initial analysis. Oxygen is nearly ubiquitous in gas-sensing and catalytic environments, and is a known electron scavenger. Oxygen can adsorb on the surfaces in several configurations. It can be adsorbed with one end of the molecule on the surface, or laying on its side on the surface. These configurations can be observed for TiO_2 in Figure 5.

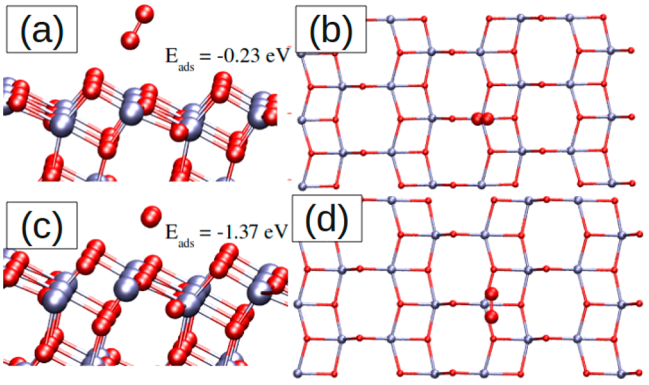

Figure 5. Stable configurations for oxygen adsorbed over the stoichiometric (101) surface of TiO_2 anatase. (a) Side view of end-on surface configuration. (b) Top view of end-on surface configuration. (c) Side view of side-on surface configuration. (d) Top view of side-on surface configuration.

We checked several configurations, and the most stable configuration over all of the metal oxides studied was with O_2 laying nearly flat on the surface (the side-on configuration in Figure 5c). This is true on both the stoichiometric and the reduced surfaces. We report adsorption energies for O_2 over both stoichiometric and reduced surfaces in Table 3. ΔE in the table is defined as the difference in adsorption energy between the reduced and stoichiometric surfaces. In previous work,[64] the adsorption energy of oxygen on a stoichiometric anatase (101) surface in the side-on configuration was calculated to be −0.90 eV and in the end-on configuration −0.58 eV, while we calculated these values to be −1.37 and −0.23 eV, respectively. Despite the difference between this previous work and our results, the trends coincide with a more stable molecule in the side-on configuration. The differences in numerical results could be possibly due to the methodologies used, as the calculations reported by Zeng et al.[64] were performed with relativistic SBJK pseudopotentials and basis set, and the B3LYP exchange correlation functional. However, Aschauer et al.[65] calculated the side-on configuration adsorption energy for a stoichiometric surface to be −1.5 eV, which is close to our value of −1.37 eV. In another work,[67] the adsorption energies were calculated using DFT methods in the generalized gradient corrected approximation (GGA) with the PBE exchange and correlation functional; the results were −2.37 eV for the side-on configuration over a reduced surface and −0.34 eV for oxygen molecule in the end-on configuration over a stoichiometric surface, which match the trend of our calculations.

We observed that adsorption is significantly enhanced over the reduced surfaces as compared to stoichiometric surfaces, as shown by the large negative values of ΔE for the side-on configuration of O_2. ΔE is the difference in adsorption energies over reduced and stoichiometric surfaces. Negative values for ΔE indicate that adsorption is preferred over reduced surfaces. Because we considered O_2 binding to cationic metal sites, charge transfer from the surface to adsorbate (giving negatively charged ionic O_2) leads to stronger binding between cationic metal and anionic O_2 (see Figure 1). The electrons available for transfer to O_2 directly result from the O_v defects, so binding is enhanced over the reduced surfaces. As we discuss below, this charge-transfer process will become more evident.

Likely the side-on configuration is most stable because it produces stronger ionic bonding between the surface and O_2; each O atom can interact with a surface metal cation (see Figure 5d). We also observed that the adsorption energy differences between the reduced and stoichiometric surfaces follow the trend $|\Delta E_{TiO2}| < |\Delta E_{ZrO2}| < |\Delta E_{HfO2}|$. More will be said of this in later sections. We examined the nature of O_2 adsorption by looking at the O−O bond lengths, which are given in Table 3. The observed bond lengthening over the reduced surfaces suggests a weakening of the O−O bond, which is indicative of charge transfer taking place between O_2 and the surface. Gas-phase O_2 has a calculated bond length of 1.22 Å, while superoxide species O_2^- has a typical bond length of 1.23 Å and peroxide species O_2^{2-} has a typical bond length of 1.48 Å.[65]The adsorbed O_2 bond lengths over reduced surfaces match the O_2^{2-} bond lengths well, while O_2 bond lengths over stoichiometric surfaces match gas-phase O_2 bond lengths. Again, the reduced surfaces have unpaired electrons available for transfer to the O_2, while the stoichiometric surfaces have no such unpaired electrons.

For comparison, we also analyzed the end-on adsorption configuration, with the molecule pointed away from the surface (and slightly bent) as is shown in Figure 5. This was the second most stable configuration over all of the metal oxides. The O_2 bond length over all surfaces (reduced and stoichiometric) for end-on adsorption was always similar to the bond length of gas-phase oxygen molecule (~1.2 Å). This suggests that large charge transfer is not occurring with the end-on configuration and weaker ionic interactions occur between O_2 in this geometry and the surface. The differences in adsorption energies over stoichiometric and reduced surfaces are all nearly zero for the end-on configuration, again suggesting little

dx.doi.org/10.1021/jp3043285 | J. Phys. Chem. C 2012, 116, 16573−16581

Table 3. Adsorption Energies (eV) and O−O Bond Lengths (Å) of Molecular Oxygen over Stoichiometric and Reduced Surfaces[a]

	side-on configuration					end-on configuration				
	stoichiometric surface		reduced surface			stoichiometric surface		reduced surface		
metal oxide	ads. energy	bond length	ads. energy	bond length	ΔE	ads. energy	bond length	ads. energy	bond length	ΔE
TiO_2	−1.37	1.24	−3.15	1.44	−1.78	−0.23	1.23	−0.24	1.23	−0.01
ZrO_2	−0.55	1.24	−3.94	1.48	−3.39	−0.18	1.22	−0.18	1.23	0
HfO_2	−1.36	1.23	−5.28	1.5	−3.91	−0.2	1.23	−0.2	1.22	0

[a] ΔE is defined as the difference in adsorption energy between the reduced and stoichiometric surfaces.

electron transfer whether over reduced or stoichiometric surfaces.

To first order, the adsorption energy can be written as:

$$E_{ads} \approx E_{electrontransfer} + E_{electrostaticinteractions} \quad (3)$$

The transfer of electrons to O_2 involves a certain positive energy cost ($E_{electron\ transfer}$) that is compensated by the favorable electrostatic interactions ($E_{electrostatic\ interactions}$) between the newly formed anion and surface cation. Thus, E_{ads} is exothermic, or negative, when $E_{electrostatic\ interactions}$ is more negative than the positive $E_{electron\ transfer}$ value. In the end-on configuration, only one O atom interacts with a surface metal cation, and thus any compensating electrostatic interactions between negatively charged O_2 and cation are minimized. Electron transfer does not occur for end-on geometry because the anionic O_2 would not be stabilized enough on the surface to overcome energetic barriers for electron transfer, or $E_{electrostatic\ interactions}$ is smaller than $E_{electron\ transfer}$. In contrast, a much larger ionic character can be assigned to O_2 in the side-on configuration (which has very favorable electrostatic interactions between both O atoms and a surface cation or large $E_{electrostatic\ interactions}$), and this is reflected by the stronger adsorption energies and bond distances of this configuration.

To confirm the charge transfer process, we also performed Bader charge analysis. Table 4 shows the charges of the oxygen

Table 4. Bader Charges (e−) of Oxygen Adsorbed over the Stoichiometric and Reduced Surfaces

metal oxide		stoichiometric	reduced
TiO_2	side-on	−0.58	−2.12
	end-on	0.01	0.01
ZrO_2	side-on	−1.16	−2.01
	end-on	0.02	−0.01
HfO_2	side-on	−0.04	−1.17
	end-on	0.01	0.01

molecule adsorbed over the stoichiometric and reduced surfaces. In all cases, the oxygen molecule over a reduced surface has a more negative charge in the side-on configuration, indicating that electrons are transferred from the surface to the O_2 molecule. The charge value near −2 is evidence of peroxide O_2^{2-} species formation . For the end-on configuration, there is negligible charge transfer. We note that defining a Bader volume to calculate Bader charges is not without difficulty, and obtaining O_2 charges to be exactly −2 is problematic with some charges slightly lower than −2. Nonetheless, the charges do show that greater charge transfer occurs over reduced surfaces. We also note that some charge transfer occurs over stoichiometric surfaces, but these electrons come from filled electronic states in the metal oxides and are much less energetically transferable than unpaired electrons in reduced surfaces. $E_{electron\ transfer}$ is very high over stoichiometric surfaces, which is why the adsorption energy is lower as compared to reduced surfaces, which have lower $E_{electron\ transfer}$.

Our results show that stronger binding occurs when O_2 becomes an anion, or when ionosorption takes place, and that this adsorption process occurs over all of the group IV metal oxides studied. The configuration of the O_2 during the adsorption process determines directly whether the ionosorption process can take place or not. This geometry dependence may have great influence on the surface chemistry of the metal oxide surfaces, especially when considering coadsorption of other molecules or higher surface adsorption coverages. These latter two effects may influence stable adsorption geometries, and hence the electron transfer process. Further research is needed to clarify the influence of coverage and coadsorbates on ionosorption over metal oxides. We next endeavor to explain the different behavior of the metal oxides considered in this study.

3.3. Comparison of O_2 Adsorption on the Different Metal Oxides. Understanding the charge-transfer processes over the various metal oxides involves several complexities, but we provide some analysis comparing the different surfaces. To discover any trends, we computed the O_v formation energy over each surface. These results are shown in Table 5. The

Table 5. Formation Energy of an Oxygen Vacancy on the Surface of the Studied Metal Oxides

metal oxide	energy [eV]
TiO_2	4.87
ZrO_2	7.14
HfO_2	7.47

most reducible of the studied surfaces is anatase, and the reducibility decreases with tetragonal ZrO_2 being more reducible than HfO_2 (101) surfaces. The reducibility is roughly a measure of the M−O bonding strength in the surface. Covalent systems would tend to have smaller vacancy formation energies. In contrast, strongly ionic systems would tend to have larger vacancy formation energies. The differences in electronegativity between O and metal atom for atomic Ti, Zr, and Hf are −1.90, −2.11, and −2.14,[66] indicating a rough order of ionic character for the metal oxides. Thus, oxides of TiO_2 are to be the least ionic, while oxides in HfO_2 are the most ionic in character. This trend is reflected in the O_V formation energies and O_2 adsorption energies. The most ionic system (HfO_2) has the strongest O_2 surface binding (−5.28 eV) due to the largest anion−cation interactions ($E_{electrostatic\ interactions}$ in eq 3). Conversely, the least ionic system (TiO_2) has the weakest adsorption energy (−3.15 eV) due to the weakest ionic interactions between the O_2 anion and Ti cation.

dx.doi.org/10.1021/jp3043285 | J. Phys. Chem. C 2012, 116, 16573−16581

The work function is also another parameter for comparison. The work function represents the energy required to remove an electron from the material (or $E_{\text{electron transfer}}$ in eq 3), and it is expected that materials with lower work functions will lead to easier/more facile electron transfer. Table 6 shows our calculated work functions for the studied metal oxides; the work function trends match the trends of O_2 adsorption over reduced surfaces very well. For example, TiO_2 has the largest work function value, so removal of electrons from TiO_2 is hardest (largest $E_{\text{electron transfer}}$), which in turn leads to the O_2 adsorption energy being the weakest. HfO_2 has the smallest work function and has the strongest (most stable) adsorption energy, indicating charge transfer is easiest for this oxide. The relative electronegativities of the surface and adsorbate have been used as key parameters to understand charge transfer between surface and adsorbate as in previous work.[3] Electrons flow from less electronegative species to more electronegative species. Thus, the difference between the electronegativity of the surface and the adsorbate is indicative of the degree or possibility of electron transfer. The absolute electronegativity can be taken approximately to be equal to the work function. We see that metal oxides with higher electronegativities (as approximated by the work function) lead to less stable ionosorption. Referring to eq 3, raising $E_{\text{electron transfer}}$ lowers the adsorption energy, or makes the process more endothermic.

Table 6. Calculated Work Functions (eV) for the Studied Metal Oxide Surfaces

metal oxide	work function
TiO_2	6.91
ZrO_2	6.31
HfO_2	6.15

We have provided two correlations that explain the trends in O_2 adsorption energy over these reduced metal oxide surfaces. The oxygen vacancy formation energy is largest for HfO_2, which indicates a strongly ionic oxide, and the adsorption energy of O_2 over HfO_2 is also most exothermic, particularly due to strong ionic bonding. HfO_2 also has the lowest work function, so removal of an electron from HfO_2 is easiest, and thus charge transfer proceeds most readily over HfO_2. These two properties of a metal oxide may be useful to predict charge-transfer behavior and trends in other metal oxides.

3.4. DFT+*U* Analysis of the Surfaces. We next tested the effect of DFT+*U* on ionosorption.[68] The prediction of delocalized defect states in anatase is not consistent with experimental data.[69,70] The need for self-interaction corrections to describe the polaronic nature of excess electrons in TiO_2 has been discussed by several authors.[18,19] Corrected computations were carried out within the DFT method modified with on-site Coulomb correction terms, or DFT+*U*. We applied a *U* value to all of the metal atoms (Ti, Zr, Hf).

Figure 6 shows the electron localized in the 3d orbitals of the Ti atoms neighboring the oxygen vacancy after applying DFT +*U* in anatase TiO_2. The oxygen vacancy gave two unpaired electrons in the oxide, and in our solution they are both localized on different Ti atoms with opposite spins.

The adsorption energies of oxygen over the reduced metal oxide surfaces using DFT+*U* and a range of *U* values are shown in Figure 7. Our results indicate little change in adsorption energies for *U* = 5 eV, but the adsorption energies increase for *U* = 8 eV. This trend is consistent with previous work.[3] At

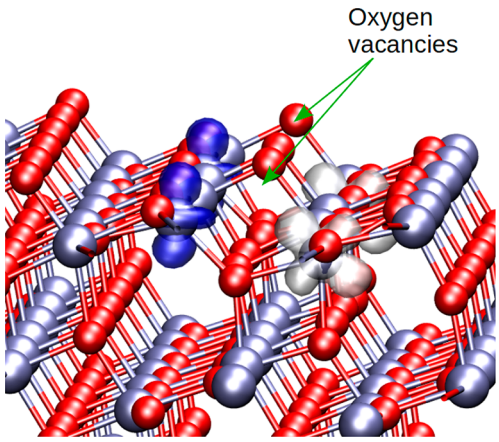

Figure 6. Electron spin density localized in the 3d orbitals of Ti atoms in anatase neighboring an oxygen vacancy using DFT+*U* with *U* = 5 eV. The white surface represents the spin up density and the blue surface the spin down density. Two unit cells are represented in the [010] direction to see the oxygen vacancies.

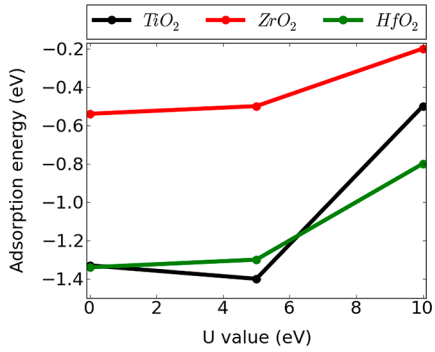

Figure 7. Adsorption energies (eV) of molecular oxygen over the reduced metal oxide surfaces using the DFT+*U* method.

sufficiently large *U* values, the transfer of electrons to the O_2 molecule becomes hindered ($E_{\text{electron transfer}}$ becomes larger) because the larger *U* values stabilize the electrons in the oxide lattice. Increasing the *U* value lowers the defect state energy location within the band gap; small *U* values give defect states near the conduction band, while large *U* values give defect states near the valence band. *U* values in between give defect states in the band gap. The *U* value becomes a way to control the unpaired electrons' stability within the lattice, and influence ionosorption. Last, DFT+*U* has the largest effect on TiO_2. Standard DFT gives solutions with delocalized electrons in TiO_2, while solutions of ZrO_2 and HfO_2 have localized states (see section 3.1). DFT+*U* has the largest effect on TiO_2 because it induces electron localization and considerably modifies the electronic nature of the unpaired electrons, much more so than in ZrO_2 and HfO_2. This modification of TiO_2 due to DFT+*U* is clearly indicated by the large change in adsorption energy at increasing *U* values.

3.5. Adsorption of Other Molecules. Previous work by one of the authors examined a variety of molecules adsorbed over the rutile (110) surface.[3] It was shown that significant electron transfer did not occur for species with low electronegativity (e.g., H_2O). The main criterion for this analysis was how the adsorption energy changed over the stoichiometric as compared to over the reduced surface. Significant change in adsorption energy would indicate electron transfer from the

dx.doi.org/10.1021/jp3043285 | J. Phys. Chem. C 2012, 116, 16573−16581

reduced surface to the adsorbate, or ionosorption taking place. We also modeled adsorption of several species over the anatase TiO_2, ZrO_2, and HfO_2 surfaces to assess how the electronegativity of the adsorbate influences the strength of adsorption.

Figure 8 shows the differences between the energy of adsorption of various species on the stoichiometric and the reduced surface for the (101) surface of the anatase phase of TiO_2. Figures 9 and 10 contain similar results for ZrO_2 and HfO_2, respectively. As before, the difference in energy of adsorption is defined as $\Delta E_{ads} = E_s - E_r$, where E_s is the energy of adsorption on the stoichiometric surface and E_r is the energy of adsorption on the reduced surface, similar to ΔE in section 3.2. Again, adsorption over cationic metal sites only was considered, because this type of binding will be most affected by electron transfer. Electronegativity values were taken from Pearson.[71]

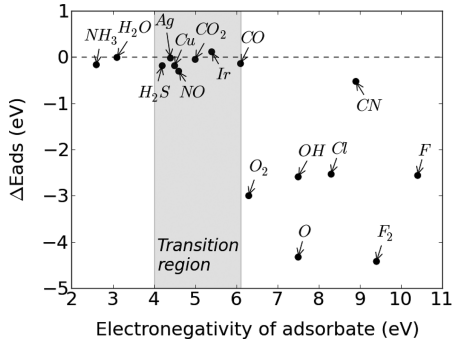

Figure 8. Differences in adsorption energies over clean and reduced surfaces (ΔE_{ads}) as a function of adsorbate electronegativity for the TiO_2 anatase (101) surface.

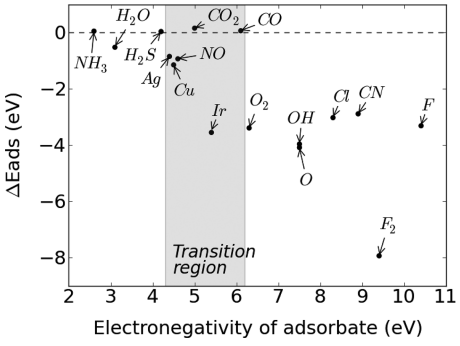

Figure 9. Differences in adsorption energies over clean and reduced surfaces (ΔE) as a function of adsorbate electronegativity for the ZrO_2 (101) surface.

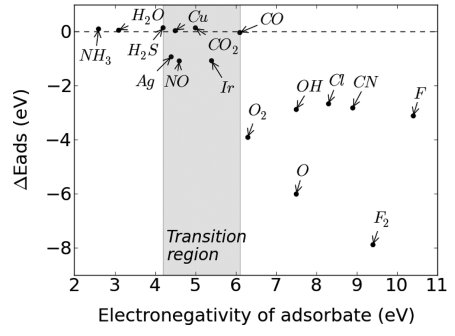

Figure 10. Differences in adsorption energies over clean and reduced surfaces (ΔE) as a function of adsorbate electronegativity for the HfO_2 (101) surface.

We observed large negative values of ΔE_{ads} for several species, which is indicative of a strong effect due to the presence of excess electrons and enhanced charge transfer over the reduced surfaces. Several species with low values of electronegativities were not affected by the reduction of the surface. A transition region (such as shown in Figure 8) indicates when ΔE_{ads} starts to become nonzero. In essence, when the electronegativity of the adsorbate is roughly lower than the electronegativity of the surface, the transfer of charge is not a favorable process, and the reduced surface behaves as a stoichiometric surface. Ionosorption does not occur, and covalent bonding is dominant. We note that the ΔE_{ads} values are stronger for anatase as compared to rutile TiO_2[3] (for example, ΔE_{ads} is −0.6 eV over rutile for atomic O, while −4.5 eV over anatase). At this point, it is very likely that the specific surface structure (e.g., coordination numbers or orbital levels) will influence the adsorption energies; generally anatase is more reactive than rutile.[25] We observed similar effects over ZrO_2 and HfO_2 (see Figures 9 and 10), in that the electronegativity value of the adsorbate is a large indicator of whether increased binding over reduced surfaces will occur.

In previous work,[3] the electronegativity of the rutile (110) surface was approximated as the work function of the surface. We find that our calculated work function values (see Table 6) do not exactly match the transition region, which we attribute to the limitations of calculating the work function as well as breakdown of the assumption that work function and electronegativity are equivalent. However, we have observed that the work functions and transition regions are relatively close, which supports the idea that adsorbates with electronegativities less than the surface electronegativities will not ionoadsorb.

Ionosorption has now been observed with four metal oxide surfaces: rutile TiO_2 (110),[3] anatase TiO_2 (101), tetragonal ZrO_2 (101), and tetragonal HfO_2 (101). We expect this to be a very general phenomena with ionic transition metal oxides, but further work needs to be performed to confirm how widespread this occurs. We have only considered O vacancy defects, but other electron-donating defects (such as interstitial atoms) likely also lead to ionosorption, as previously observed.[3] Clearly, defects may strongly affect surface adsorption and surface chemistry in several different ways, and thus any theoretical modeling of these surfaces should take into account the possibility of ionosorption. For example, simply using a stoichiometric slab may lead to wrong results with electronic structure calculations. Furthermore, there is also much experimental work focusing on understanding defects and their role in oxide surface chemistry, and certainly future research will provide more details on metal oxide ionosorption.

4. CONCLUSIONS

We have presented evidence that suggests ionosorption should occur over group IV metal oxides (TiO_2, ZrO_2, and HfO_2) with electron-donating defects. Increased binding of O_2 is observed when the surface is reduced and unpaired electrons are present in the surface slab. These electrons transfer to O_2 forming an anion that may favorably interact with surface metal cations. This electron transfer process is dependent on the adsorption geometry, as we observed that not all stable O_2 adsorption

dx.doi.org/10.1021/jp3043285 | J. Phys. Chem. C 2012, 116, 16573−16581

modes lead to electron transfer. We have examined the details of the ionosorption over the different metal oxides, and two parameters correlate with the adsorption energies of O_2: surface vacancy formation energy and surface work function. HfO_2 has the largest O vacancy formation energy of the studied oxides, but also has the most exothermic O_2 adsorption energy, which is explained by the larger ionic nature of HfO_2. Larger ionic character will lead to stronger binding between the cationic metal sites and anionic adsorbates. HfO_2 also has the lowest work function, which indicates that electron transfer from HfO_2 is easiest. Correspondingly, anatase TiO_2 has the lowest O vacancy formation energy, the largest work function, and the least exothermic O_2 adsorption energy. Increased binding is also observed for several other adsorbates, but only when the adsorbate electronegativity is significantly large, which indicates that the electronegativity of the adsorbate should be larger than the electronegativity of the surface. Certainly, our results reinforce the idea that electrons and charge transfer are important when surface chemistry over early transition metal oxides is studied, and future work may examine this concept over other metal oxides.

AUTHOR INFORMATION

Corresponding Author

*E-mail: nadeskins@wpi.edu.

Notes

The authors declare no competing financial interest.

ACKNOWLEDGMENTS

Computational resources were provided by the Molecular Science Computing Facility at the Environmental Molecular Science Laboratory of Pacific Northwest National Laboratory. Battelle operates the Pacific Northwest National Laboratory for the U.S. Department of Energy.

REFERENCES

(1) Diebold, U.; Li, S. C.; Schmid, M. *Annu. Rev. Phys. Chem.* **2010**, *61*, 129−148.
(2) Lira, E.; Wendt, S.; Huo, P.; Hansen, J. Ø.; Streber, R.; Porsgaard, S.; Wei, Y.; Bechstein, R.; Lægsgaard, E.; Besenbacher, F. *J. Am. Chem. Soc.* **2011**, *133*, 6529−6532.
(3) Deskins, N. A.; Rousseau, R.; Dupuis, M. *J. Phys. Chem. C* **2010**, *114*, 5891−5897.
(4) Wendt, S.; Sprunger, P. T.; Lira, E.; Madsen, G. K. H.; Li, Z.; Hansen, J. Ø.; Matthiesen, J.; Blekinge-Rasmussen, A.; Lægsgaard, E.; Hammer, B. *Science* **2008**, *320*, 1755−1759.
(5) Martinez, U.; Hammer, B. *J. Chem. Phys.* **2011**, *134*, 194703 1−7.
(6) Madsen, G. K. H.; Hammer, B. *J. Chem. Phys.* **2009**, *130*, 044704 1−7.
(7) Chretien, S.; Metiu, H. *J. Chem. Phys.* **2008**, *128*, 0447141−13.
(8) Hoffmann, M. R.; Martin, S. T.; Choi, W.; Bahnemann, D. W. *Chem. Rev.* **1995**, *95*, 69−96.
(9) Diebold, U. *Surf. Sci. Rep.* **2003**, *48*, 53−229.
(10) Henderson, M. A.; Epling, W. S.; Peden, C. H. F.; Perkins, C. L. *J. Phys. Chem. B* **2002**, *107*, 534−545.
(11) Petrik, N. G.; Kimmel, G. A. *J. Phys. Chem. Lett.* **2010**, *1*, 1758−1762.
(12) Barsan, N.; Schweizer-Berberich, M.; Göpel, W. *Fresenius' J. Anal. Chem.* **1999**, *365*, 287−304.
(13) Wang, C.; Yin, L.; Zhang, L.; Xiang, D.; Gao, R. *Sensors* **2010**, *10*, 2088−2106.
(14) Gurlo, A. *ChemPhysChem* **2006**, *7*, 2041−2052.
(15) Nanto, H.; Minami, T.; Takata, S. *J. Appl. Phys.* **1986**, *60*, 482−484.
(16) Ahn, M.-W.; Park, K.-S.; Heo, J.-H.; Park, J.-G.; Kim, D.-W.; Choi, K. J.; Lee, J.-H.; Hong, S.-H. *Appl. Phys. Lett.* **2008**, *93*, 263103 1−3.
(17) Tao, Y.; Cao, X.; Peng, Y.; Liu, Y. *Sens. Actuators, B* **2010**, *148*, 292−297.
(18) Pacchioni, G. *J. Chem. Phys.* **2008**, *128*, 182505 1−10.
(19) Ganduglia-Pirovano, M. V.; Hofmann, A.; Sauer, J. *Surf. Sci. Rep.* **2007**, *62*, 219−270.
(20) Linsebigler, A. L.; Lu, G.; Yates, J. T. *Chem. Rev.* **1995**, *95*, 735−758.
(21) Lu, G.; Linsebigler, A.; Yates, J. J. T. *J. Chem. Phys.* **1995**, *102*, 4657−4662.
(22) Chi, L. P.; Lindsay, R.; Thornton, G. *Chem. Soc. Rev.* **2008**, *37*, 2328−2353.
(23) Dohnálek, Z.; Lyubinetsky, I.; Rousseau, R. *Prog. Surf. Sci.* **2010**, *85*, 161−205.
(24) Zapol, P.; Curtiss, L. A. *J. Comput. Theor. Nanosci.* **2007**, *4*, 222−230.
(25) Sclafani, A.; Herrmann, J. M. *J. Phys. Chem.* **1996**, *100*, 13655−13661.
(26) Vittadini, A.; Selloni, A.; Rotzinger, F. P.; Grätzel, M. *Phys. Rev. Lett.* **1998**, *81*, 2954−2957.
(27) Vittadini, A.; Casarin, M.; Selloni, A. *Theor. Chem. Acc.* **2007**, *117*, 663−671.
(28) Miller, K. L.; Musgrave, C. B.; Falconer, J. L.; Medlin, J. W. *J. Phys. Chem. C* **2011**, *115*, 2738−2749.
(29) Liu, L.-M.; Li, S.-C.; Cheng, H.; Diebold, U.; Selloni, A. *J. Am. Chem. Soc.* **2011**, *133*, 7816−7823.
(30) Gong, X.-Q.; Selloni, A.; Dulub, O.; Jacobson, P.; Diebold, U. *J. Am. Chem. Soc.* **2007**, *130*, 370−381.
(31) Luo, X.; Demkov, A. A.; Triyoso, D.; Fejes, P.; Gregory, R.; Zollner, S. *Phys. Rev. B* **2008**, *78*, 2453141−10.
(32) Fiorentini, V.; Gulleri, G. *Phys. Rev. Lett.* **2002**, *89*, 266101 1−4.
(33) Chen, R.; Kim, H.; McIntyre, P. C.; Bent, S. F. *Appl. Phys. Lett.* **2004**, *84*, 4017−4019.
(34) Stenzel, O.; Wilbrandt, S.; Schürmann, M.; Kaiser, N.; Ehlers, H.; Mende, M.; Ristau, D.; Bruns, S.; Vergöhl, M.; Stolze, M.; et al. *Appl. Opt.* **2011**, *50*, C69−C74.
(35) Giorgi, G.; Korkin, A.; Yamashita, K. *Comput. Mater. Sci.* **2008**, *43*, 930−937.
(36) Peacock, P. W.; Robertson, J. *Phys. Rev. Lett.* **2004**, *92*, 057601 1−4.
(37) Robertson, J. *Rep. Prog. Phys.* **2006**, *69*, 327−396.
(38) Iskandarova, I. M.; Knizhnik, A. A.; Rykova, E. A.; Bagatur'yants, A. A.; Potapkin, B. V.; Korkin, A. A. *Microelectron. Eng.* **2003**, *69*, 587−593.
(39) Syzgantseva, O.; Calatayud, M.; Minot, C. *J. Phys. Chem. C* **2010**, *114*, 11918−11923.
(40) Añez, R.; Sierraalta, A.; Martorell, G.; Sautet, P. *Surf. Sci.* **2009**, *603*, 2526−2531.
(41) Hofmann, A.; Ganduglia-Pirovano, M. V.; Sauer, J. *J. Phys. Chem. C* **2009**, *113*, 18191−18203.
(42) Wang, C.-M.; Fan, K.-N.; Liu, Z.-P. *J. Am. Chem. Soc.* **2007**, *129*, 2642−2647.
(43) Haase, F.; Sauer, J. *J. Am. Chem. Soc.* **1998**, *120*, 13503−13512.
(44) Foster, A. S.; Sulimov, V. B.; Lopez Gejo, F.; Shluger, A. L.; Nieminen, R. M. *Phys. Rev. B* **2001**, *64*, 224108 1−10.
(45) Zheng, J. X.; Ceder, G.; Maxisch, T.; Chim, W. K.; Choi, W. K. *Phys. Rev. B* **2007**, *75*, 104112 1−7.
(46) Pietrucci, F.; Bernasconi, M.; Laio, A.; Parrinello, M. *Phys. Rev. B* **2008**, *78*, 094301 1−7.
(47) VandeVondele, J.; Krack, M.; Mohamed, F.; Parrinello, M.; Chassaing, T.; Hutter, J. *Comput. Phys. Commun.* **2005**, *167*, 103−128.
(48) Lippert, G.; Hutter, J.; Parrinello, M. *Theor. Chem. Acc.* **1999**, *103*, 124−140.
(49) VandeVondele, J.; Hutter, J. *J. Chem. Phys.* **2007**, *127*, 114105.
(50) Goedecker, S.; Teter, M.; Hutter, J. *Phys. Rev. B* **1996**, *54*, 1703−1710.

(51) Hartwigsen, C.; Goedecker, S.; Hutter, J. *Phys. Rev. B* **1998**, *58*, 3641−3662.
(52) Krack, M. *Theor. Chem. Acc.* **2005**, *114*, 145−152.
(53) Perdew, J. P.; Burke, K.; Ernzerhof, M. *Phys. Rev. Lett.* **1997**, *78*, 1396−1396.
(54) Horn, M.; Schwerdtfeger, C.; Meaghe, E. *Z. Kristallogr.* **1972**, *136*, 273−281.
(55) Teufer, G. *Acta Crystallogr.* **1962**, *15*, 1187−1188.
(56) Adams, D. M.; Leonard, S.; Russell, D. R.; Cernik, R. J. *J. Phys. Chem. Solids* **1991**, *52*, 1181−1186.
(57) Fall, C. J.; Binggeli, N.; Baldereschi, A. *J. Phys.: Condens. Matter* **1999**, *11*, 2689−2696.
(58) Bader, R. *Atoms in Molecules: A Quantum Theory (International Series of Monographs on Chemistry)*; Oxford University Press: New York, 1994.
(59) Tang, W.; Sanville, E.; Henkelman, G. *J. Phys.: Condens. Matter* **2009**, *21*, 084204 1−7.
(60) Sanville, E.; Kenny, S. D.; Smith, R.; Henkelman, G. *J. Comput. Chem.* **2007**, *28*, 899−908.
(61) Henkelman, G.; Arnaldsson, A.; Jónsson, H. *Comput. Mater. Sci.* **2006**, *36*, 354−360.
(62) Cheng, H.; Selloni, A. *Phys. Rev. B* **2009**, *79*, 0921011−4.
(63) Safonov, A. A.; Bagatur'yants, A. A.; Korkin, A. A. *Microelectron. Eng.* **2003**, *69*, 629−632.
(64) Zeng, W.; Liu, T.; Wang, Z.; Tsukimoto, S.; Saito, M.; Ikuhara, Y. *Mater. Trans.* **2010**, *51*, 171−175.
(65) Aschauer, U.; Chen, J.; Selloni, A. *Phys. Chem. Chem. Phys.* **2010**, *12*, 12956−12960.
(66) Lide, D. *CRC Handbook of Chemistry and Physics*; CRC Press: Maryland, 2004.
(67) Mattioli, G.; Filippone, F.; Amore Bonapasta, A. *J. Am. Chem. Soc.* **2006**, *128*, 13772−13780.
(68) Dudarev, S. L.; Botton, G. A.; Savrasov, S. Y.; Humphreys, C. J.; Sutton, A. P. Electron-energy-loss spectra and the structural stability of nickel oxide: An LSDA+U study. *Phys. Rev. B* **1998**, *57* (3), 1505−1509.
(69) Berger, T.; Sterrer, M.; Diwald, O.; Knözinger, E.; Panayotov, D.; Thompson, T. L.; Yates, J. T. *J. Phys. Chem. B* **2005**, *109*, 6061−6068.
(70) Zhou, S.; Čižmár, E.; Potzger, K.; Krause, M.; Talut, G.; Helm, M.; Fassbender, J.; Zvyagin, S. A.; Wosnitza, J.; Schmidt, H. *Phys. Rev. B* **2009**, *79*, 113201 1−4.
(71) Pearson, R. G. *Inorg. Chem.* **1988**, *27*, 734−740.